Biosensors and Bioelectronics 41 (2013) 736–744

Contents lists available at SciVerse ScienceDirect

Biosensors and Bioelectronics

journal homepage: www.elsevier.com/locate/bios

# Parallel recording of neurotransmitters release from chromaffin cells using a 10 × 10 CMOS IC potentiostat array with on-chip working electrodes

Brian N. Kim [a,b,*], Adam D. Herbst [a], Sung J. Kim [c], Bradley A. Minch [d], Manfred Lindau [a]

[a] School of Applied and Engineering Physics, Cornell University, Ithaca, NY 14853, USA
[b] Graduate Field of Biophysics, Cornell University, Ithaca, NY 14853, USA
[c] School of Electrical Engineering and Computer Science, Seoul National University, Seoul 151–742, South Korea
[d] Franklin W. Olin College of Engineering Needham, MA 02492, USA

ARTICLE INFO

*Article history:*
Received 28 June 2012
Received in revised form
14 September 2012
Accepted 27 September 2012
Available online 5 October 2012

*Keywords:*
Amperometry
Biosensor
Electrochemical recording
High throughput
On-chip recording
Post-fabrication

ABSTRACT

Neurotransmitter release is modulated by many drugs and molecular manipulations. We present an active CMOS-based electrochemical biosensor array with high throughput capability (100 electrodes) for on-chip amperometric measurement of neurotransmitter release. The high-throughput of the biosensor array will accelerate the data collection needed to determine statistical significance of changes produced under varying conditions, from several weeks to a few hours. The biosensor is designed and fabricated using a combination of CMOS integrated circuit (IC) technology and a photolithography process to incorporate platinum working electrodes on-chip. We demonstrate the operation of an electrode array with integrated high-gain potentiostats and output time-division multiplexing with minimum dead time for readout. The on-chip working electrodes are patterned by conformal deposition of Pt and lift-off photolithography. The conformal deposition method protects the underlying electronic circuits from contact with the electrolyte that covers the electrode array during measurement. The biosensor was validated by simultaneous measurement of amperometric currents from 100 electrodes in response to dopamine injection, which revealed the time course of dopamine diffusion along the surface of the biosensor array. The biosensor simultaneously recorded neurotransmitter release successfully from multiple individual living chromaffin cells. The biosensor was capable of resolving small and fast amperometric spikes reporting release from individual vesicle secretions. We anticipate that this device will accelerate the characterization of the modulation of neurotransmitter secretion from neuronal and endocrine cells by pharmacological and molecular manipulations of the cells.



## 1. Introduction

The electrochemical recording of biomolecules has a wide range of applications: from biomedical sensing, with implanted electrodes in a living animal's brain to detect the level of dopamine (DA) release (Kissinger et al., 1973), to biophysical applications where it is used to understand the membrane fusion mechanism, called exocytosis, mediating neurotransmitter release (Wightman et al., 1991; Chow et al., 1992; Bruns and Jahn, 1995; Chow and Rüden, 1995; Pothos et al., 1998). Some neurotransmitters, such as DA, epinephrine (adrenaline), norepinephrine (noradrenaline), and serotonin, are oxidized by a polarizable electrode held at ~700 mV vs. an Ag|AgCl reference electrode, and the resulting electron transfer is measurable using a current-to-voltage amplifier. Polarizable electrodes have high electrolyte/electrode interface resistance that introduces negligible background current. Thus, the oxidation (faradic) current can be closely monitored with high signal-to-noise ratio, a technique called amperometry. Neurotransmitters are released in packets or quanta from vesicles that fuse with the cell membrane, which can be detected as an amperometric spike (Wightman et al., 1991; Chow et al., 1992). The amperometric spike provides the precise amount and time course of released molecules in a single vesicle fusion event and thereby details of the vesicle–plasma membrane fusion process. The total charge that is collected from a single vesicle release (quantal size) is closely related to the volume of the vesicle (Van der Kloot and Molgo, 1994; Finnegan et al., 1996; Albillos et al., 1997; Bruns et al., 2000), because the neurotransmitter concentration inside the vesicles is relatively constant (Colliver et al., 2000b; Gong et al., 2003). A so-called foot signal preceding the steep amperometric spike (Chow et al., 1992) indicates neurotransmitter

* Corresponding author at: Cornell University, School of Applied and Engineering Physics, 187 Clark Hall, Ithaca, NY 14853, USA. Tel.: +1 607 255 0632; fax: +1 607 255 6032.
*E-mail addresses:* bnk25@cornell.edu (B.N. Kim), adh38@cornell.edu (A.D. Herbst), kimsj@snu.ac.kr (S.J. Kim), Bradley.Minch@olin.edu (B.A. Minch), ml95@cornell.edu (M. Lindau).

0956-5663/$ - see front matter © 2012 Elsevier B.V. All rights reserved.
http://dx.doi.org/10.1016/j.bios.2012.09.058

leaking through a narrow fusion pore at the initial step of exocytosis (Albillos et al., 1997; Gong et al., 2007). Based on this understanding of the biophysical mechanisms that determine the features of the amperometric spike, amperometry can be used to identify the effects of drugs on vesicle fusion in living cells. Amperometric recordings have revealed that quantal size is increased by the Parkinson's drug L-Dopa and decreased by drugs such as reserpine (Pothos et al., 1996; Kozminski et al., 1998; Pothos et al., 1998). Alternatively, treatment with drugs such as botulinum toxin A (Botox) appears to influence the rate of release events, and the properties of the fusion pore, without affecting quantal size (Criado et al., 1999; Fang et al., 2008).

Amperometric spikes vary in their properties, such as half-width, foot signal, and amplitude, from cell to cell even when they are measured from the same cell type under the same condition (Colliver et al., 2000a). In order to identify the effect of a drug on secretory cells, a large number of single cell measurements must therefore be performed to determine statistical significance of a change in the mean value. Conventional amperometric recordings are performed with a carbon fiber microelectrode positioned close to a single cell using a micromanipulator under microscopic observation. Not only is the equipment costly, but an expert performing the cell recordings one by one will need to spend a long time to gather enough recordings to derive conclusions with statistical significance.

Such limitations may be overcome by development of a scalable electrochemical detector array in which the working electrodes are integrated with the amplifiers. Amplifier and sensor integration using CMOS technology has been used in different biosensing applications to reduce the size of the biosensor system but still sustain the high-quality performance of conventional systems (Pancrazio et al., 1998; DeBusschere and Kovacs, 2001; Heer et al., 2004; Heer et al., 2007; Rothe et al., 2011). For amperometric recordings of quantal release, a low-noise CMOS potentiostat using a shared amplifier structure has been developed (Ayers et al., 2007) onto which suitable polarizable electrode materials can be deposited (Ayers et al., 2010).

Here, we present an electrochemical biosensor array with a large number of electrode–amplifier pairs. This biosensor can simultaneously measure the quantal release of oxidizable transmitters from many cells cultured on-chip. The high-throughput capability provides a great benefit to both biomedical and biophysical applications. In biomedical implants, this biosensor could provide a spatially resolved image of a DA release. As a biophysical research instrument, its parallel amplifier circuit–electrode pairs would allow large numbers of single-cell recordings to be performed simultaneously. The application of high-throughput electrochemical sensors arrays will drastically accelerate the elucidation of the mechanisms of transmitter release and their modulation by drug treatments.

## 2. Material and methods

### 2.1. CMOS fabrication

The CMOS IC incorporating a $10 \times 10$ array of potentiostats as well as timing and readout circuitry (Fig. 1a) was designed in

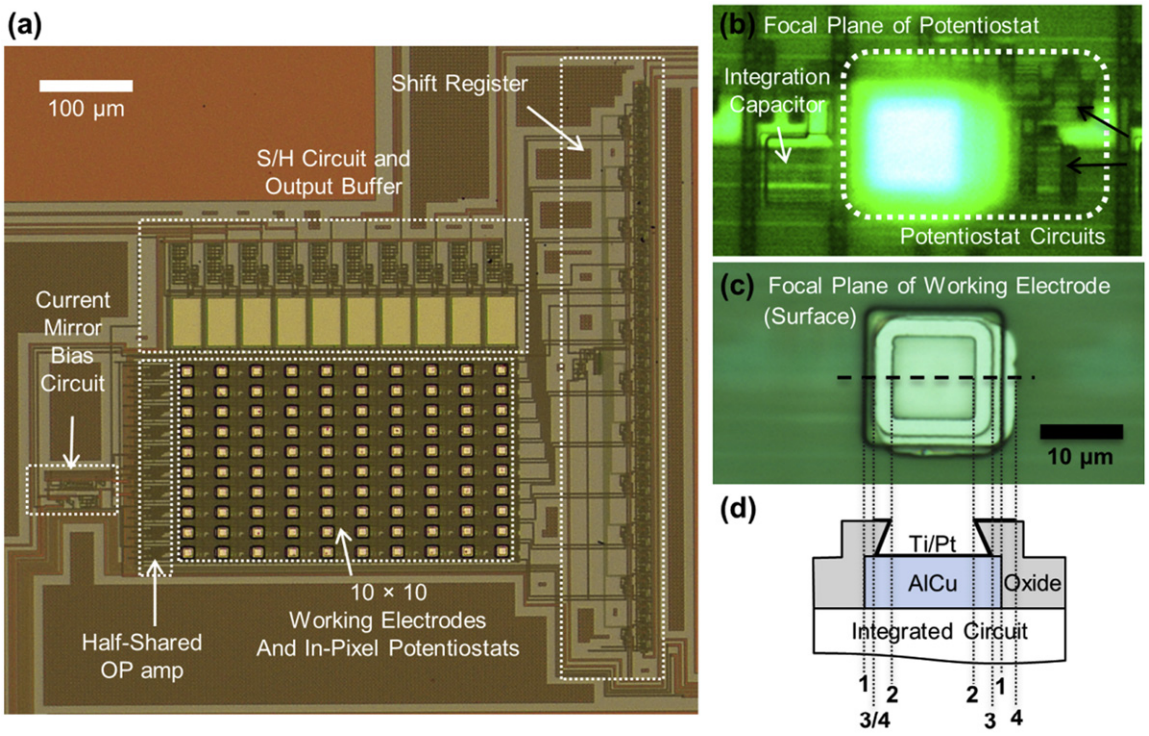


**Fig. 1.** Amperometric amplifier array. (a) Photograph of chip surface with working electrodes and underlying circuitry after post-fabrication. The $10 \times 10$ electrode array was visible as bright squares; each electrode was $15\ \mu m \times 15\ \mu m$ in size. Each in-pixel potentiostat contains only a half of an operational amplifier taking advantage of a half-shared operational amplifier design. The shift register controlled the timing of the S/H circuit to multiplex the electrode outputs per each column of 10 electrodes. (b) and (c) are microphotographs of individual electrode/potentiostat array element at different focal planes. The focal plane of (b) was at the underlying potentiostat, consisting of 9 transistors (two of which are indicated by black arrows) and an integrating capacitor that converted the recording current to voltage. The focal plane of (c) was at the surface working electrode above the potentiostat. (d) Schematic of electrode topology. $15\ \mu m \times 15\ \mu m$ AlCu contacts served as interconnection between the surface patterned Pt electrode and the potentiostat. The overglass has $10\ \mu m \times 10\ \mu m$ openings at the top with an undercut expanding to a $\sim 12\ \mu m \times 12\ \mu m$ area of exposed AlCu. The thick black line, atop AlCu and Oxide, indicates the area covered by Ti/Pt. The cross section along the horizontal dashed line is shown schematically in (c). The vertical dotted lines indicate the edges of the AlCu contacts (1), the overglass opening (2), the undercut (3), and the slightly misaligned bright area where Pt is patterned (4).

Tanner Tools EDA, simulated using H-Spice with parameters for On Semiconductor C5F/N, and the design submitted for fabrication through MOSIS. The On Semiconductor C5F/N (previously known as AMIS 0.5 μm) process does not offer a polarizable electrode material such as gold or platinum among the options of metal layer materials. Therefore, 15 μm × 15 μm AlCu contacts were included in the design to serve as interconnection between the electrode material and the underlying integrated amplifier shown in Fig. 1b. Using a half-shared operational amplifier design (Ayers et al., 2007), one potentiostat circuit consisted of only 9 transistors and one capacitor for the oxidation charge integration that is small enough to be positioned under an electrode. To deposit Pt directly onto these contacts, the design included 10 μm × 10 μm openings in the overglass layer in register with the AlCu contacts. Due to the aggressive etching process, these openings had an undercut structure as shown in Figs. 1c, d.

### 2.2. Post-fabrication of Pt electrodes

For the post-fabrication of the Pt electrodes each 3 mm × 3 mm die was attached to a 25 mm × 25 mm glass coverslip (VWR micro cover glass) with epoxy (DOUBLE/BUBBLE Epoxy, HARDMAN) to facilitate handling and to prevent damage by electrostatic discharge. After cleaning the surface of the IC and coverslip with acetone and isopropanol, positive photoresist S1813 (Shipley) was spin-coated onto the surface at 4000 rpm for 30 s and baked on a hotplate at 90 °C for 1 min. Using an ABM contact aligner and a negative toned mask, the pattern for the Pt electrodes was transferred to the photoresist on the IC by UV exposure. The die/coverslip was then placed in a YES Image Reversal Oven with ammonia gas, exposed to UV light for 60 s, and developed for 60 s in MF-321, which removed the photoresist where Pt would be deposited and left the photoresist elsewhere as a sacrificial layer. Following Pt deposition (see below) this sacrificial layer was removed (Photoresist Remover 1165) leaving the patterned Pt electrode array, with the surface between the electrodes insulated by the overglass layer.

Due to the undercut in the openings exposing the AlCu contacts unidirectional Pt vapor deposition resulted in imperfect coverage of the exposed AlCu contacts by Pt. As a consequence, electrolyte could make low resistance contact with the AlCu, leading to excessive currents. To achieve complete coverage of the AlCu contacts, conformal electron beam physical vapor deposition of 15 nm titanium and 100 nm Pt was performed using a rotating shelf. This process introduced multiple angles of incidence to the incoming vapor of metal atoms, resulting in complete coverage of the AlCu contacts and created a continuous Ti/Pt layer at the side wall of the overglass openings as well as the sacrificial photoresist layer on top. To avoid the formation of rough edges of the Pt at the edges of the overglass openings during lift-off of the sacrificial layer, the openings in the photoresist defining the Pt covered areas were slightly larger (15 μm × 15 μm) than the overglass openings such that small defects at the edges of the Pt electrode would not impact the chip's performance. A schematic of the geometry with an aligned image of a single electrode of the array (Fig. 1c) is shown on an expanded scale in Fig. 1d.

### 2.3. Packaging

The die was mounted on a side-braze Dual in-line Package (Addison Engineering, San Jose, California, USA) using 5 min Epoxy (Devcon) and wire bonded (Fig. 2a). To prevent contact of the electrolyte with the contact pads and wire bonds, these areas were insulated with silicone (RTV 615, GE) (Fig. 2b). The chip carrier with the mounted die was placed on a heated metal block during the application of silicone accelerating the curing process to prevent flow of silicone to the center of the IC where the working electrodes must remain exposed for direct contact with cells and the electrolyte.

### 2.4. Solutions and DA application

The standard solution contained 140 mM NaCl, 5 mM KCl, 1 mM $MgCl_2$, 10 mM $CaCl_2$, and 10 mM HEPES/NaOH (pH 7.3) with the osmolality adjusted to 300 mmol/kg by adding glucose. The high $K^+$ stimulating solution contained 140 mM KCl, 5 mM NaCl, 1 mM $MgCl_2$, 10 mM $CaCl_2$, and 10 mM HEPES/NaOH (pH 7.3) with the osmolality adjusted to 300 mmol/kg by adding glucose. The electrode array was covered with 40–100 μL of standard solution and DA was injected from a pipette adding 10 μL of standard solution containing DA at high concentration (0.35–5.3 mM). For measurements of the DA concentration dependence, the electrode array was covered with 40–90 μL of the standard solution and 10 μL of DA solution was rapidly mixed into the solution to reach final concentrations of 350 nM, 3.5 μM, 35 μM, 70 μM, and 105 μM.

### 2.5. Cell preparation and culture on the biosensor

Bovine adrenal glands were obtained from a local slaughter house and chromaffin cells were cultured in 70 mL cell culture flasks as described (Parsons et al., 1995). After one day of incubation at 37 °C and 10% $CO_2$, the cells were suspended and plated on the Poly-D-Lycine (0.05%) coated biosensor (Fig. 2c). The biosensor array with the cell cultured was incubated for another ~24 h before recordings were made. Shortly before the recording, the cell culture media atop the biosensor was exchanged with 50 μL of the standard solution. For stimulation of neurotransmitter secretion, 50 μL of the stimulating solution was added to the standard solution, resulting in a final concentration of 70 mM of KCl.

### 2.6. Electrochemical recording, data acquisition and analysis

After an Ag|AgCl reference electrode was inserted into the bath and connected to ground, power was supplied to the chip along with the clock signals. Initially, the potentiostat outputs were saturated due to the capacitive currents charging the electrode capacitance to 700 mV, followed by a slow decay to a very small stable baseline current within 1 min. The analog output signals were digitized by a 16-bit analog-to-digital converter (ADC) (PCI-6251 and PXIe-6368, National Instruments, Austin, TX) using Igor Pro 6, Wavemetrics for data acquisition and a user written procedure for de-multiplexing and data analysis. The time windows during which the signals from each electrode were presented at the output pins were 25 μs long and a sampling rate of 500 kS/s per output (column with 10 electrodes) was used to acquire the signals from all 10 columns (100 electrodes). When only one column of electrodes was recorded a sampling rate of 1 MS/s was used. The recordings were low pass filtered digitally in IGOR PRO by 5-s binomial smoothing for the DA injection experiments and by 10-ms binomial smoothing for the live-cell recordings. Data analysis for live-cell experiment was performed using Quanta Analysis software as described (Mosharov and Sulzer, 2005).

## 3. Results

### 3.1. Amperometric amplifier array

Amperometric detection of DA and other catecholamines is typically performed by a current measurement applying ~700 mV holding potential to a polarizable working electrode relative to an

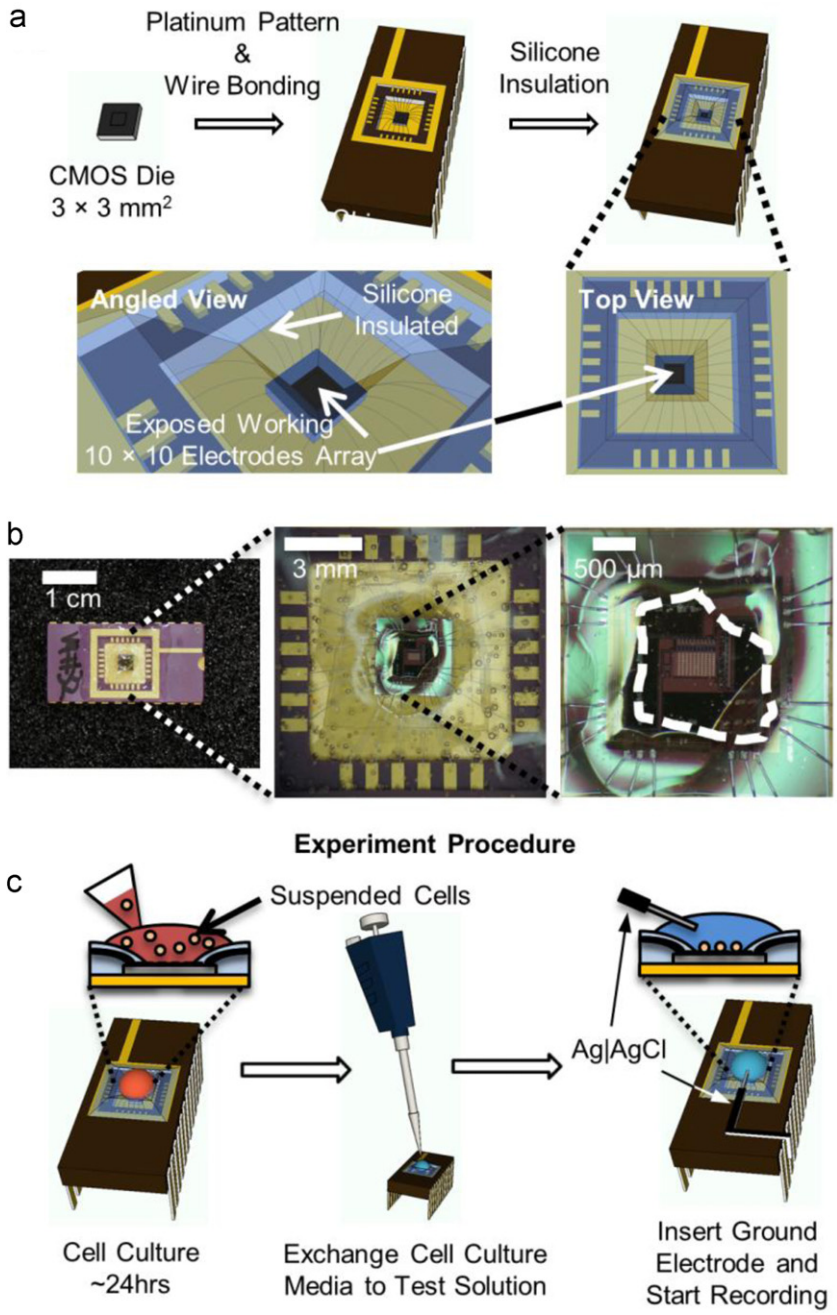


**Fig. 2.** Packaging of the amperometric chip and live-cell experiment procedure. (a) A $3 \times 3$ mm$^2$ CMOS die with post-fabricated Pt electrodes was wire bonded to a chip carrier. Silicone was applied at the surface of the chip carrier insulating the wire bonds and contact pads. This only left the center of the CMOS die exposed where the working electrode array was located. (b) Photograph of IC biosensor package with silicone insulation of wire bonds and contact pads. The area of the IC that was exposed without silicone coverage is indicated by the white dashed line. The amperometric amplifier array shown in Fig. 1a was located at the center of this exposed area. (c) Schematically shown experiment procedure from the cell culture on the chip to the live-cell recording.

Ag|AgCl reference electrode that was inserted into the electrolyte and connected to the ground. The array shown in Fig. 1a incorporated an array of potentiostats (Ayers et al., 2007) connected to surface patterned Pt working electrodes and arranged in 10 rows × 10 columns.

DA molecules making contact with the electrode are oxidized, transferring two electrons per molecule to the electrode. The arrival of DA molecules thus produces an oxidation current that passes through the potentiostat circuit and is integrated on a 50-fF capacitor ($C_{charge}$, Fig. 3a) resulting in a voltage signal, $V_n$, which is read out every sampling period as a value $V_{sn}$ at the end of the integration period. The faradic current from the oxidation of catecholamine molecules in individual release events from chromaffin cells (Wightman et al., 1991) can be up to 500 pA in amplitude but foot signals indicating fusion pore properties (Chow et al., 1992) require a resolution of $<10$ pA. To resolve currents in this range, we have chosen an amplifier gain of $\sim 10$ mV/pA. To resolve the time course of individual release events a sampling rate of 2 kS/s per electrode is typically used. The rms noise of the potentiostat is $\sim 100$ fA (Ayers et al., 2007), comparable to that of conventional low-noise amplifiers. In practice, conventional amperometric carbon-fiber electrodes act

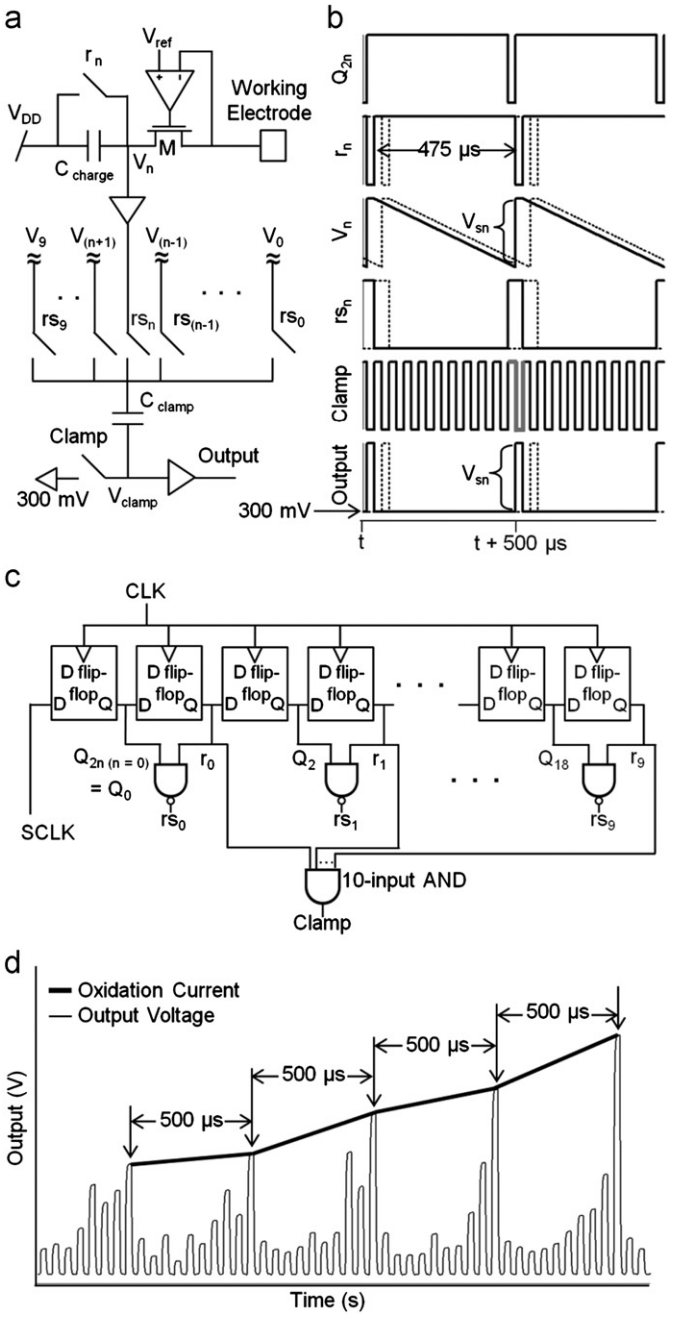


**Fig. 3.** Time-division multiplexing of amperometric current measurements from 10 sensors ($n$=0…9) in a column. (a) Potentiostat circuit and multiplexer. The oxidation current at the working electrode charges $C_{charge}$ decreasing $V_n$ over the integration period, which is set to 475 µs by clock $r_n$ that reset $V_n$ back to $V_{DD}$ (5V). At the end of integration cycle, $rs_n$ switch closes and connects $V_n$ to $C_{clamp}$. $C_{clamp}$ is an AC coupling capacitor that removes the DC component in $V_n$, and is controlled by the on/off cycle of the Clamp switch. After this cycle, the $rs_{(n+1)}$ switch is closed and couples $V_{(n+1)}$ through $C_{clamp}$ to the output. This is repeated to multiplex all the outputs in a time-division fashion. (b) Timing signals, time course of voltage $V_n$ at $C_{charge}$ and the final output signal $V_{sn}$ representing the total amount of charge collected during the integration period. (c) Subclock generation timing circuit generates reset clocks ($r_n$), row selection clocks ($r_{sn}$) that is produced using $Q_{2n}$ and $r_n$, and a clamp clock (Clamp). (d) Example output from one column of electrodes, illustrating the de-multiplexing process. The output was recorded with a 1-µs sampling interval. The trace starts with the data from the electrode of row 0, followed by that of row 1, and so on. Extracting the values at the times indicated by arrows provides the time course of the current measured by the electrode in row 7 (thick black line).

as antennas picking up excess noise, which is minimized in the microchip technology presented here, because the Pt electrodes are patterned directly on top of the IC.

### 3.2. Multiplexing outputs from a large number of parallel acquisitions

When a large number of parallel electrode–amplifier pairs were incorporated, the main challenge becomes to sample all the data in parallel and transfer them to a computer for storage and analysis. We used a time-division multiplexing approach to limit the number of outputs from the chip to be sampled by the computer to 10 (1 per column), and staggered the integration periods for the capacitors along a column, so that, while one amplifier is being read out, all the other potentiostats in the column continue to integrate their respective input currents. Thus, each potentiostat integrated its input current for 95% of the sampling interval (475 µs/sample), interrupted by 25-µs readout and reset periods.

During the 475-µs integration interval, the oxidation current entering through the potentiostat decreased $V_n$ as electrochemically transferred electrons fill $C_{charge}$. At the end of the sampling interval, the reset clock $r_n$ goes low, resetting $V_n$ to $V_{DD}$ (Fig. 3b). The change in $V_n$ at the end of the integration period ($V_{sn}$) represents the inverse of the total charge collected during 475-µs with an offset voltage of $V_{DD}$. The polarity of $V_{sn}$ is reversed and the offset adjusted using capacitor $C_{clamp}$ and the clamp switch. All the voltages $V_0$.$V_9$ are in parallel, such that the row selection signal $r_{sn}$ carries $V_n$ to $C_{clamp}$. At the end of the integration period, the clamp switch is closed by the high clamp signal (Fig. 3b, Clamp - gray line) to reset $V_{clamp}$ to a default voltage, in this case 300 mV. At the time of the reset of $V_n$ to $V_{DD}$, the Clamp clock goes low (gray line) to take $V_{sn}$ to $V_{clamp}$ such that the decrease in $V_n$ over the 475 µs integration period is transferred to $V_{clamp}$ as an increase. In this way, all outputs in a column are serially presented at a single output through time-division multiplexing (Fig. 3b dashed lines). $V_{clamp}$ is read out through an output buffer to lower the output impedance. The IC was operated from a main clock (CLK, 40 kHz and 50% duty cycle) and a sampling clock (SCLK, 2 kHz and 95% duty cycle). From these clocks the timing circuitry in the IC derives the subclocks (Fig. 3c). As shown in Fig. 3c, SCLK enters a shift register, a series of D flip-flops, to produce the reset signals (i.e., $r_0$,…, $r_9$) for resetting each row's $C_{charge}$ capacitor. The reset signals are identical to SCLK except for a delay of 2n (where n is the row number) times the 25-µs CLK period. As shown in Fig. 3c, a row selection signal for row n ($r_{sn}$) is generated using a two-input NAND gate whose inputs are $r_n$ and $Q_{2n}$ (i.e., the subclock that precedes $r_n$ by a period of CLK).

An example stream of output data from an individual column is shown in Fig. 3d. Data from all 10 electrodes appear sequentially in a 500-µs time interval. The multiplexed output was demultiplexed after sampling by the computer. In the current implementation the signal from row 0 was identified by recording SCLK and aligning it with the column output, using the known delay for each row selection ($r_{sn}$) relative to SLCK. The thick line in Fig. 3d illustrates the extraction of the signal $V_{s7}$ as an example of output demultiplexing. It represents the time course of the current that was measured at the electrode located in row 7, with a sampling rate of 2 kS/s. Likewise the signals from all rows were extracted and saved separately for further analysis.

### 3.3. Device validation by dopamine sensing

DA is readily oxidized in amperometric recordings with surface patterned Pt microelectrodes (Berberian et al., 2009) and the sensor array was tested measuring the electron transfer induced by DA application (Fig. 4a). Fig. 4b shows the current from an electrode in column 9 in response to DA addition to a final concentration of ~70 µM. The measured current level

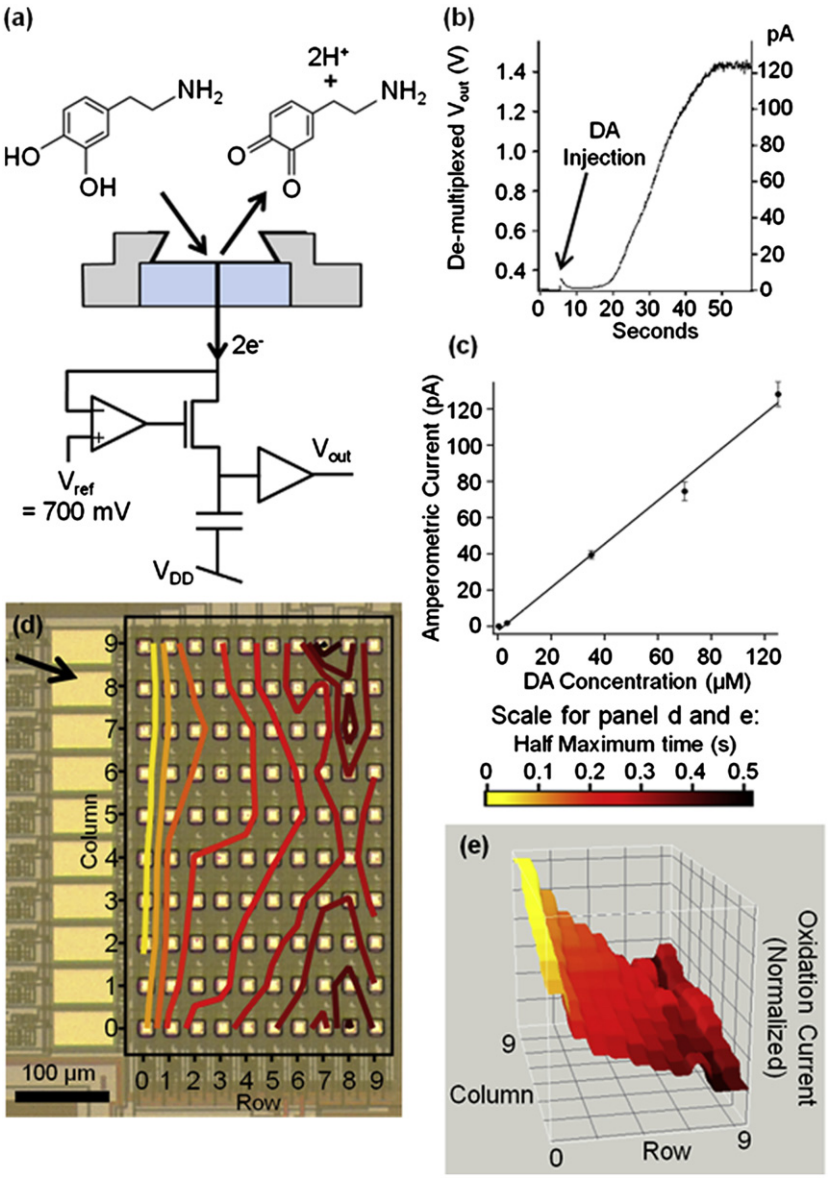


**Fig. 4.** (a) Scheme of DA recording concept. At the surface of an electrode that is held at 700 mV, a DA molecule makes contact with the platinum through diffusion and is oxidized, transferring 2 electrons to the electrode and leaving DA-o-quinone to diffuse away. $V_{out}$ changes as the charges that enter the electrode pass through the potentiostat circuit and are collected at the capacitor. (b) Oxidation current from an electrode initially covered with 40 μL of standard solution after injection of 10 μL standard solution containing 350 μM DA. (c) DA concentration dependence of average currents. Data points are averaged from all 100 electrode of the $10 \times 10$ electrode array. The error bars are SEM. The slope of linear fit was 1.20 pA/μM. (d, e) Representations of DA response from 100-electrode array. Following a single injection of DA, all electrodes reported oxidation currents and the half maximum times of the dopamine responses are plotted for every electrode according to its position. Time 0 was defined as the time where the electrode in column 9, row 0, was half saturated. (d) Photograph indicating the orientation of the electrode array and the direction of DA diffusion from the injection site (arrow). Colored contour lines indicate half maximum times of current at each electrode. (e) Three-dimensional DA concentration profile measured from all 100 electrodes simultaneously at $t=200$ ms. The $z$-axis is the normalized oxidation current measured from the electrode array to best visualize the diffusional wave of DA. Colors indicate half maximum times for individual electrodes as in (d).

showed a slow increase after DA injection to ~120 pA reflecting the diffusional DA to the electrodes.

Application of DA at final concentrations of 350 nM, 3.5 μM, 35 μM, 70 μM, and 105 μM in the bath solution, produced oxidation currents at the 100 electrodes. The current change measured from each electrode was quantified by taking the difference between first and last point of 0.2 Hz smoothed recordings of 60 s duration. Data from all 100 electrodes were averaged to determine the average current change for each DA concentration. The average current of the 100 electrodes increased linearly with DA concentration in the range 3.5–105 uM with a slope of 1.20 pA/μM (Fig. 4c). The lowest concentration that we could reliably detect was 0.35 μM giving an average current of $0.1 \pm 0.06$ pA (s.d.). The average responses of the different electrodes in the array were $39.5 \pm 23.2$ pA (s.d.) in the presence of 35 μM and $128.2 \pm 67.5$ (s.d) in the presence of 105 μM DA. Such variability is presumably in part due to differences in area between the different electrodes but is in part also due to variations in DA concentration due to overlapping diffusion layers as has been shown for DA sensing by a passive carbon ring microelectrode array (Lin et al., 2012). The calibration of amplifier gain was tested by direct current injection into the surface electrode (held at 700 mV) via a 10 GΩ resistor connected to ground for each of the 10 electrodes in a single column. The average from the 10 electrodes was $76.7 \pm 2.6$ pA s.d., indicating that the variability of gain between different electrodes is $< 3.5\%$.

Corresponding measurements with two other biosensor arrays provided slopes of 0.95 and 0.90 pA/μM. These small variations are presumably due to the variations in the active size of the electrodes, which result from separate die-based post-fabrications. The variability will be reduced in wafer-based post-fabrication. It should be noted that the values of 0.95 and 0.90 pA/μM were obtained with two different devices on the same day with the same solutions, whereas the 1.2 pA/μM slope was obtained on a different day with a different freshly prepared DA solution. Given the instability of DA, differences in actual DA concentration may have contributed to the apparent differences in sensitivity.

The observed variability between electrodes and between different arrays does not affect the measurement of single vesicle release events because the individual release sites are in close contact with the sensor and have dimensions that are almost 100 times smaller than the electrodes ensuring complete oxidation of all released molecules.

The functionality of the full 100-electrode array was further demonstrated by injecting DA at a final concentration of ~500 μM, which eventually saturated the potentiostats. For a graphical representation of the electrode responses, the time where the current recorded by a particular electrode reached its half saturation value was coded in gray scale in Fig. 4d. Fig. 4e shows a contour plot of half saturation times for the different electrodes of the array, visualizing the flow of DA over the surface of the electrode array. These plots indicate that DA molecules initially appeared at the upper left side of the electrode array. The electrode in column 9, row 0, showed the most rapid response, very closely followed by its neighboring electrodes as the DA diffused toward the lower electrodes. The time course of the currents recorded by all 100 electrodes reflecting DA diffusion was fully revealed in a Video of the DA concentration profile (see Supplementary Data). Fig. 4f shows DA concentration profile at $t=200$ ms from the video, showing the wave of DA reaching the electrodes and eventually saturating the potentiostats.

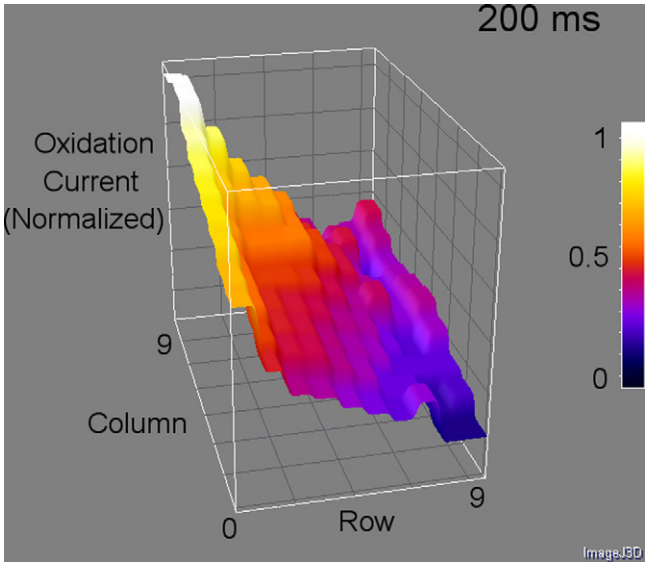


**Video S1.** Video representation of three-dimensional DA concentration profile measured from all 100 electrodes simultaneously. The *xy*-plane represents the spatial arrangement of the electrode array. The *z*-axis and color indicate the normalized oxidation current response from the electrodes. Time 0 was defined as the time where the electrode in column 9, row 0, was half saturated. The diffusion of DA is shown from the time course of the three-dimensional representation. The arrival of DA from the upper left corner, column 9, row 0, was followed by the diffusion of DA toward lower right corner, creating a shape of wave in the video. Supplementary material related to this article can be found online at http://dx.doi.org/10.1016/j.bios.2012.09.058.

### 3.4. Amperometric recording of transmitter release

To demonstrate the live-cell measurement of single vesicle release events, chromaffin cells were cultured on the biosensor for 24 h (Fig. 5). The chip provided stable baseline currents $<100$ pA after up to 3 days with cultured cells in the incubator, which corresponds to a nominal electrode resistance of 7 GΩ. The chip provided stable currents after up to 3 days with cultured cells in the incubator. Typical cell sizes are $<20$ μm but some cell aggregates of larger size are also present. Out of the 12 electrodes shown in Fig. 5, 8 electrodes were fully or partially covered by chromaffin cells. After a high $K^+$ stimulation, amperometric events were recorded by most of cell-covered electrodes as well as adjacent electrodes. Each amperometric spike corresponds to quantal release of the contents from a single vesicle and its integral is proportional to the number of released molecules (quantal size). In Fig. 5, the amperometric traces are plotted at the spatial locations of the respective electrodes. The electrode with a single cell atop (column 2 × row 3) recorded fast amperometric spikes with ~10 ms half-width. For this electrode, two spikes are shown on an expanded scale, one with 14.8-pA amplitude and 11-ms half-width and the other with 1.6-pA amplitude and 40-ms half-width which was the smallest spike recorded by this electrode. The quantal size ranged from 0.1 pC to 1.2 pC with an average of 0.49 pC These values agree well those previously reported for carbon-fiber experiments on bovine chromaffin cells (Wightman et al., 1991; Chow et al., 1992), indicating that the sensor readily detects the released molecules. With 2 electrons transferred per molecule, a quantal size of 0.1 pC corresponds to ~300,000 molecules. The noise in the recordings was ~0.15 pA rms at 100 Hz bandwidth. We estimate that release events down to ~6000 molecules should be detectable.

The other electrodes with cell aggregates on them detected spikes that had half-width $>100$ ms, which was presumably caused

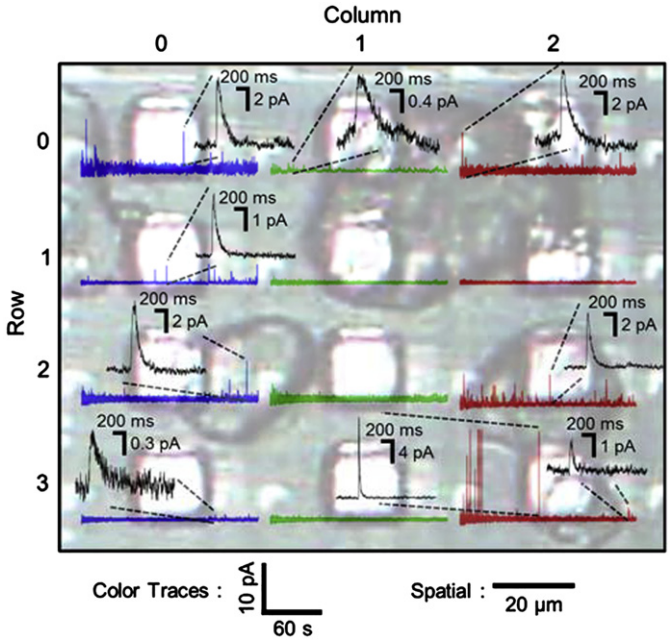


**Fig. 5.** Live chromaffin cell recording of neurotransmitter release. Chromaffin cells were cultured on-chip 24 h prior to the recording. Photograph showing 12 of 100 electrodes partly covered with cells atop. Cells were stimulated by 70 mM KCl. The amperometric traces from each electrode are superimposed. Black traces show individual events on expanded scale depending on individual amperometric spike amplitudes. The size of an individual cell (column 2, row 3) was typically $<20$ μm. Aggregated cells that is $>20$ μm were found on column 0 × row 1–row 2, column 1 × row 0–row 1, and column 2 × row 0–row 2 electrodes.

by the diffusional broadening that reflects the increased traveling distance before released molecules reached the electrode (Schroeder et al., 1992; Hafez et al., 2005). Accordingly, electrodes (column 0 × row 0 and row 3) without direct contact to a cell recorded spikes that were very small and slow, presumably originated from release events of distant cells. This parallel recording of amperometric spikes confirmed the biosensor's capability to record quantal release events simultaneously from live-cells over the typical recording time (~150 s) with sub-millisecond resolution, pico-ampere current resolution, and stability without a significant baseline drift over time that is comparable to conventional low-noise amplifiers. In some cases, such as the electrode in column 1 - row 1, no amperometric spikes were recorded although a cell appeared to be present over the electrode. The absence of amperometric spikes could simply be explained by inactivity of the cell. However, it should be noted that this electrode was covered by part of a cell aggregate such that the space between a chromaffin cell and the electrode may have been obstructed by other material preventing rapid diffusion of released molecules from the cell surface to the electrode.

## 4. Discussion

Neurotransmitter release occurs in the form of quanta from vesicles that fuse with the cell membrane. The amount and time course of release can be recorded as an amperometric spike using microelectrodes Amperometric recordings revealed that quantal size is increased by the Parkinson's drug L-Dopa and decreased by reserpine (Pothos et al., 1996; Kozminski et al., 1998; Pothos et al., 1998). Treatment with botulinum toxin A (Botox) reduces the rate of release events, and changes the properties of the fusion pore, without affecting quantal size (Criado et al., 1999; Fang et al.,2008). It is of great interest to develop a high-throughput technology to characterize the modulation of transmitter release by drugs or molecular manipulations.

The array presented here is optimized primarily for recording of single vesicle release events. By their nature, these events originate from vesicles ~200 nm in diameter and the released molecules produce a finite charge and current. The ideal electrode has therefore a size that is similar to the size of the cell to maximize the capture of release events from the cell surface. Our design incorporates such cell-sized microelectrodes. Larger electrodes produce increased noise (Yao and Gillis, 2012) but not a larger signal and therefore reduced signal-to-noise ratio. For this reason recordings of single release events are generally performed with microelectrodes.

In recent years, planar microelectrode arrays have been fabricated for the measurement of quantal release using different materials to create polarizable electrodes suitable for amperometric recordings. These include platinum (Dias et al., 2002; Berberian et al., 2008), pyrolyzed photoresist (Zachek et al., 2009), carbon (Zhang et al., 2008; Lin et al., 2012), ITO (Kisler et al., 2012), nitrogen-doped diamond-like carbon (DLC:N) (Barizuddin et al., 2010), boron-doped nanocrystalline diamond (Carabelli et al., 2010) and organic polymers (Yang et al., 2011). The limitation of such microelectrode arrays is that for parallel recordings each electrode needs to be connected to an external amplifier, and such devices are therefore not scalable. Few attempts have been made to integrate polarizable electrochemical electrodes with a potentiostat array on-chip (Zhang et al., 2005; Kruppa et al., 2010; Li et al., 2011). Only one of these devices allowed simultaneous measurement from multiple electrodes, but the synchronous integration and readout periods produced a minimum 3.2 ms dead time during readout of the array (Kruppa et al., 2010). The time-division multiplexing we demonstrate here reduces the readout dead time by more than two orders of magnitude to 25 μs. Furthermore, the half-shared amplifier structure we use here (Ayers et al., 2007) reduces the area of the repeating amplifier unit to 0.0009 $mm^2$, which approaches cellular dimensions and makes the technology truly scalable. To our knowledge, we demonstrate for the first time the simultaneous on-chip recording of quantal release events from living cells on a 100-electrode array.

Amperometric spike time course, amplitude and charge can be affected by the diffusion distance between the release site and the amperometric electrode as has been shown for carbon fiber microelectrodes (Wightman et al., 1995). Release events from an area of a cell that is not in direct contact with the electrode will produce smaller and slower amperometric spikes due to diffusion (Hafez et al., 2005). The results of Fig. 5 show that single release events with rapid amperometric spikes are successfully recorded when a single cell adheres to an electrode, whereas cell aggregates produce smaller and slower amperometric spikes, presumably reflecting hindered diffusion. This limitation may be overcome by incorporating features that improve targeting of individual cells to individual electrodes using chemical or mechanical cues as shown in (Barizuddin et al., 2010; Liu et al. 2011). Cells located between electrodes could generate small and slow amperometric spikes at adjacent electrodes, if the adjacent electrode is not covered by another cell. Increasing spacing between electrodes would not necessarily help. Recording of amperometric spikes distorted by diffusional broadening will be minimized by improved electrode coverage by effective cell targeting.

In addition to the single cell measurements the scalable array presented here may be used to obtain spatial information of DA release in the brain. A recent publication (Zachek et al., 2010) describes a linear microelectrode array comprising four carbon-fiber microelectrodes spaced 250 μm apart that revealed heterogeneous DA release in the striatum of anesthetized rats. While the device we describe here is not designed for fast scan cyclic voltammetry, such a modification will be possible. The ability to include hundred or even more electrodes on a chip with ~1 mm dimensions would provide enhanced spatial resolution for the characterization of the spatiotemporal dynamics of DA release.

Chromaffin cells release adrenaline or noradrenaline and the use of Pt electrodes with a potential of 700 mV ensures detection of both transmitters with equal efficiency. However, specific functionalization of individual electrodes for detection of other compounds, in particular pathogens that are not per se oxidizable, would be possible (Palchetti and Mascini, 2008). The main limitation of such biosenseors is the generation of nonspecific currents by different electroactive compounds leading to potential interferences (Arora et al., 2011). The array technology described here would allow inclusion of several differently functionalized electrodes together with a number of non-functionalized "control electrodes" to distinguish specific and non-specific responses.

## 5. Conclusions

In this work, we presented an electrochemical biosensor array with high throughput capability. It incorporated an array of low-noise CMOS potentiostats using a shared amplifier structure with very small footprint area (Ayers et al., 2007). We have shown here that conformal deposition of Pt, as a polarizable electrode material was a robust process allowing on-chip application of aqueous solutions and parallel measurements of oxidizable transmitters from 100 electrodes. The biosensor allowed on-chip cell culture of 3 days in the incubator preceding stimulation and amperometric recordings. The recordings had low stable baseline values for the recording time of up to 5 min. Time-resolved measurements of the oxidation currents induced by DA injection demonstrate the

ability of this amperometric detector array to record simultaneously with all 100 electrodes. The device shows dose response linearity and could spatially resolve the current traces indicating the diffusion path of the molecules. Results from live-cell amperometry demonstrated the functionality of this biosensor's application for analysis of quantal release events with a sensitivity of ~6,000 molecules. The pico-ampere current resolution and the effective time resolution of 500 μs are suitable to resolve single vesicle secretion events from chromaffin cells. The amperometric spike parameters recorded with this array were consistent with previous carbon fiber recordings (Wightman et al., 1991; Chow et al., 1992).

## Acknowledgments

The authors thank Joan S. Lenz for her flawless technical assistance during this research, Qinghua Fang for the culture of chromaffin cells, and Sunitha Ayers for comments on the manuscript. Post-fabrication was performed in Cornell Nanofabrication Facility (CNF) and Nanobiotechnology Center (NBTC) at Cornell University, Ithaca, NY. The IC design and simulations were done in Tanner Tools EDA software. Electrostatic discharge (ESD) protection pad design was taken from the Tanner Tools design library. This work was supported by National Institutes of Health (NIH) grants R01MH095046, and T32GM008267, and National Science Foundation Agreement no. DGE-0654112 (IGERT program) administered by the Nanobiotechnology Center at Cornell University.

## References

Albillos, A., Dernick, G., Horstmann, H., Almers, W., Alvarez de Toledo, G., Lindau, M., 1997. Nature 389 (6650), 509–512.
Arora, P., Sindhu, A., Dilbaghi, N., Chaudhury, A., 2011. Biosensors and Bioelectronics 28 (1), 1–12.
Ayers, S., Gillis, K.D., Lindau, M., Minch, B.A., 2007. IEEE Transactions on Circuits and Systems I, Regular Papers 54 (4), 736–744.
Ayers, S., Berberian, K., Gillis, K.D., Lindau, M., Minch, B.A., 2010. IEEE Transactions on Biomedical Circuits and Systems 4 (2), 86–92.
Barizuddin, S., Liu, X., Mathai, J.C., Hossain, M., Gillis, K.D., Gangopadhyay, S., 2010. ACS Chemical Neuroscience 1 (9), 590–597.
Berberian, K., Kissler, K., Fang, Q., Lindau, M., 2008. Biophysical Journal 94, 1295. (1_MeetingAbstracts).
Berberian, K., Kisler, K., Fang, Q., Lindau, M., 2009. Analytical Chemistry 81 (21), 8734–8740.
Bruns, D., Jahn, R., 1995. Nature 377, 62–65.
Bruns, D., Riedel, D., Klingauf, J., Jahn, R., 2000. Neuron 28 (1), 205–220.
Carabelli, V., Gosso, S., Marcantoni, A., Xu, Y., Colombo, E., Gao, Z., Vittone, E., Kohn, E., Pasquarelli, A., Carbone, E., 2010. Biosensors and Bioelectronics 26 (1), 92–98.
Chow, R.H., Rüden, L.v., Neher, E., 1992. Nature 356, 60–63.
Chow, R.H., Rüden, L.v., 1995. Electrochemical Detection of Secretion from Single Cells. In: Sakmann, B., Neher, E. (Eds.), Single Channel Recording, 2nd ed Plenum Press, New York, pp. 245–275.
Colliver, T.L., Hess, E.J., Pothos, E.N., Sulzer, D., Ewing, A.G., 2000a. Journal of Neurochemistry 74 (3), 1086–1097.
Colliver, T.L., Pyott, S.J., Achalabun, M., Ewing, A.G., 2000b. The Journal of Neuroscience 20 (14), 5276–5282.
Criado, M., Gil, A., Viniegra, S., Gutierrez, L.M., 1999. Proceedings of the National Academy of Sciences of the United States of America 96 (13), 7256–7261.
DeBusschere, B.D., Kovacs, G.T., 2001. Biosensors and Bioelectronics 16 (7–8), 543–556.
Dias, A.F., Dernick, G., Valero, V., Yong, M.G., James, C.D., Craighead, H.G., Lindau, M., 2002. Nanotechnology 13, 285–289.
Fang, Q., Berberian, K., Gong, L.W., Hafez, I., Sorensen, J.B., Lindau, M., 2008. Proceedings of the National Academy of Sciences of the United States of America 105 (40), 15388–15392.
Finnegan, J.M., Pihel, K., Cahil, P.S., Huang, L., Zerby, S.E., Ewing, A.G., Kennedy, R.T., Wightman, R.M., 1996. Journal of Neurochemistry 66, 1914–1923.
Gong, L.W., Alvarez De Toledo, G., Lindau, M., 2003. Journal of Neuroscience 23 (21), 7917–7921.
Gong, L.W., de Toledo, G.A., Lindau, M., 2007. Nature Cell Biology 9 (8), 915–922.
Hafez, I., Kisler, K., Berberian, K., Dernick, G., Valero, V., Yong, M.G., Craighead, H.G., Lindau, M., 2005. Proceedings of the National Academy of Sciences of the United States of America 102 (39), 13879–13884.
Heer, F., Franks, W., Blau, A., Taschini, S., Ziegler, C., Hierlemann, A., Baltes, H., 2004. Biosensors and Bioelectronics 20 (2), 358–366.
Heer, F., Hafizovic, S., Ugniwenko, T., Frey, U., Franks, W., Perriard, E., Perriard, J.C., Blau, A., Ziegler, C., Hierlemann, A., 2007. Biosensors and Bioelectronics 22 (11), 2546–2553.
Kisler, K., Kim, B.N., Liu, X., Berberian, K., Fang, Q., Mathai, C.J., Gangopadhya, S., Gillis, K.D., Lindau, M., 2012. Journal of Biomaterials and Nanobiotechnology 3 (2), 243–253.
Kissinger, P.T., Hart, J.B., Adams, R.N., 1973. Brain Research 55 (1), 209–213.
Kozminski, K.D., Gutman, D.A., Davila, V., Sulzer, D., Ewing, A.G., 1998. Analytical Chemistry 70 (15), 3123–3130.
Kruppa, P., Frey, A., Kuehne, I., Schienle, M., Persike, N., Kratzmueller, T., Hartwich, G., Schmitt-Landsiedel, D., 2010. Biosensors and Bioelectronics 26 (4), 1414–1419.
Li, L., Liu, X.W., Qureshi, W.A., Mason, A.J., 2011. IEEE Transactions on Biomedical Circuits and Systems 5 (5), 439–448.
Lin, Y., Trouillon, R., Svensson, M.I., Keighron, J.D., Cans, A.S., Ewing, A.G., 2012. Analytical Chemistry 84 (6), 2949–2954.
Liu, X., Barizuddin, S., Shin, W., Mathai, C.J., Gangopadhyay, S., Gillis, K.D., 2011. Analytical Chemistry 83 (7), 2445–2451.
Mosharov, E.V., Sulzer, D., 2005. Nature Methods 2 (9), 651–658.
Palchetti, I., Mascini, M., 2008. Analytical and Bioanalytical Chemistry 391 (2), 455–471.
Pancrazio, J.J., Bey Jr., P.P., Loloee, A., Manne, S., Chao, H.C., Howard, L.L., Gosney, W.M., Borkholder, D.A., Kovacs, G.T., Manos, P., Cuttino, D.S., Stenger, D.A., 1998. Biosensors and Bioelectronics 13 (9), 971–979.
Parsons, T.D., Coorssen, J.R., Horstmann, H., Almers, W., 1995. Neuron 15 (5), 1085–1096.
Pothos, E., Desmond, M., Sulzer, D., 1996. Journal of Neurochemistry 66, 629–636.
Pothos, E.N., Davila, V., Sulzer, D., 1998. The Journal of Neuroscience 18 (11), 4106–4118.
Rothe, J., Lewandowska, M.K., Heer, F., Frey, O., Hierlemann, A., 2011. Journal of Micromechanics and Microengineering 21, 5.
Schroeder, T.J., Jankowski, J.A., Kawagoe, K.T., Wightman, R.M., Lefrou, C., Amatore, C., 1992. Analytical Chemistry 64, 3077–3083.
Van der Kloot, W., Molgo, J., 1994. Physiological Reviews 74 (4), 899–991.
Wightman, R.M., Jankowski, J.A., Kennedy, R.T., Kawagoe, D.T., Schroeder, T.J., Leszczyszyn, D.J., Near, J.A., Diliberto jr., E.J., Viveros, O.H., 1991. Proceedings of the National Academy of Sciences of the United States of America, pp 10754–10758.
Wightman, R.M., Schroeder, T.J., Finnegan, J.M., Ciolkowski, E.L., Pihel, K., 1995. Biophysical Journal 68, 383–390.
Yang, S.Y., Kim, B.N., Zakhidov, A.A., Taylor, P.G., Lee, J.K., Ober, C.K., Lindau, M., Malliaras, G.G., 2011. Advanced Materials 23 (24), H184–188.
Yao, J., Gillis, K.D., 2012. Analyst 137 (11), 2674–2681.
Zachek, M.K., Takmakov, P., Moody, B., Wightman, R.M., McCarty, G.S., 2009. Analytical Chemistry 81 (15), 6258–6265.
Zachek, M.K., Takmakov, P., Park, J., Wightman, R.M., McCarty, G.S., 2010. Biosensors and Bioelectronics 25 (5), 1179–1185.
Zhang, B., Adams, K.L., Luber, S.J., Eves, D.J., Heien, M.L., Ewing, A.G., 2008. Analytical Chemistry 80 (5), 1394–1400.
Zhang, J., Huang, Y., Trombly, N., Yang, C., Mason, A., 2005. Sensors, 2005 IEEE, pp. 385–388.